Oxidation of Metals, Vol. 36, Nos. 1/2, 1991

The Oxidation of Iron–Chromium–Manganese Alloys at 900°C

A. L. Marasco* and D. J. Young*

Received November 19, 1990

The oxidation of nine ternary iron–chromium–manganese alloys was studied at 900°C in an oxygen partial pressure of 26.7 kPa. The manganese concentration was set at 2, 6, and 10 wt.%, and chromium at 5, 12, and 20 wt.%. The scales formed on the low-chromium alloys consisted of $(Mn,Fe)_2O_3$, α-Fe_2O_3, *and* Fe_3O_4. *These alloys all exhibited internal oxidation and scale detachment upon cooling. The scales formed on the higher-chromium alloys were complicated by nodule formation. Initially, these scales had an outer layer of* $MnCr_2O_4$ *with* Cr_2O_3 *underneath, adjacent to the alloy. With the passage of time, however, nodules formed, and the overall reaction rate increased. This tendency was more marked at higher manganese contents. Although these alloys contained a high chromium content, the product chromia scale usually contained manganese. It was concluded that the presence of manganese in iron–chromium alloys had an adverse effect on the oxidation resistance over a wide range of chromium levels.*

KEY WORDS: bixbyite; iron–chromium–manganese alloys; spinel; oxidation.

INTRODUCTION

It has been shown that the addition of manganese to chromia-forming, iron–chromium alloys has an adverse effect on the oxidation resistance.[1,2,7–9,11] This is due to the fact that MnO is thermodynamically more stable than Cr_2O_3, and more importantly, that manganese has a higher diffusivity than

*School of Materials Science and Engineering, The University of New South Wales, P.O. Box 1, Kensington NSW 2033, Australia.

0030-770X/91/0800-0157$06.50/0

chromium in iron-based alloys at elevated temperatures, leading to the formation of nonprotective oxides.

Many workers have studied the effects of manganese additions at low levels on the oxidation resistance of M–Cr alloys (where M is Fe, Ni, or Co). The scales produced depended on the bulk chromium concentration. These studies involved the addition of up to 5 wt.% manganese to alloys containing approximately 20 wt.% chromium, conditions which were found to lead to the formation of $MnCr_2O_4$.[4–6] Most work on ferrous alloys has concerned the effects on oxidation kinetics of manganese additions not exceeding 5 wt.%, with the chromium content usually in excess of 25 wt.%.

As Caplan *et al.*[2] explained, at long oxidation times the manganese would rapidly diffuse from the underlying alloy, causing severe local depletion until the alloy manganese flux was reestablished. Thus, for example, once the initial manganese-enriched oxide scale had formed on an Fe–26Cr–1Mn alloy, the underlying alloy adjacent to the oxide would have a transient composition approximating to Fe–26Cr, and the chromium content would be sufficient to produce Cr_2O_3. In most studies, it was shown that $MnCr_2O_4$ would form at the gas–scale interface. With time, this outermost spinel would thicken as a result of manganese diffusion through Cr_2O_3. It was calculated that manganese cations diffused faster than chromium cations in chromia,[3] although the rate-controlling step was considered[1] to be the formation of Cr_2O_3.

The other group of iron–chromium–manganese alloys studied to date contained chromium levels considered to be subcritical for Cr_2O_3 formation. The alloys studied were Fe–9.5Cr–17.8Mn,[7] Fe–19.6Cr–15.1Mn,[8] and Fe–18Cr–12.3Mn.[9] This work indicated that a higher chromium concentration was required (greater than those used in nickel-containing stainless steels) in order to produce a chromia scale, when the alloy contained these levels of manganese. It has been reported,[11,14] that only a few tenths of a percent of manganese leads to the formation of $MnCr_2O_4$, when added to a binary iron–chromium alloy. The spinels that formed on the high-chromium alloys[8,9] varied in nature with position in the scale: iron-rich Fe–Mn spinel at the gas–scale boundary and $(Fe, Mn, Cr)_3O_4$ at the alloy-scale boundary. As for the low-chromium alloy studied,[7] the formation of manganowustite was enhanced by the fact that the amount of chromium was insufficient to destabilize the wustite phase.

The alternative possibility of an austenitic manganese-based steel is not promising. The high levels of manganese necessary to stabilize austenite in a steel containing moderate levels of chromium mean that the formation of manganese-containing spinel will be promoted. It has been observed in another alloy system[10] that the rapid diffusion of manganese caused by the oxidation of Fe–31Mn–9Al–3Cr–0.87C alloy was so extensive that a ferritic sublayer was produced beneath the scale.

The present study has been undertaken to determine the oxidation kinetics and scale morphology on ferritic Fe–Cr–Mn alloys at 900°C. Attention has been directed toward alloy compositions not previously studied: low-chromium levels with low and intermediate manganese levels, and a barely stable chromia-former again with low and intermediate manganese levels.

EXPERIMENTAL PROCEDURE

The alloys were melted from high-purity metals in a DC arc furnace with a nonconsumable tungsten electrode, under a flowing argon atmosphere. The 20 g ingots were sectioned and remelted three times to ensure mixing and then annealed at 1100°C for 24 hr in a flowing argon atmosphere. The chemical compositions of the alloys are recorded in Table I.

Samples were cut and metallographically polished to a 1 μm finish prior to oxidation. Separate experiments were performed for kinetics measurements and metallographic examination, mainly because the oxides had a propensity for spallation. The kinetics measurements were conducted using a Cahn RG electrobalance, which was encapsulated in a sealed-glass system fitted with a silica reaction tube. Samples were individually attached to a platinum hook and then suspended in the reaction tube on a silica thread attached to the electrobalance. The system was then evacuated, prior to establishing an oxygen partial pressure of 26.7 kPa. The oxidizing atmosphere was medically pure oxygen dried by passage through a column of molecular sieve. The temperature of the furnace was maintained at 900 ± 3°C. Each run commenced when the furnace was raised over the reaction tube to place the sample in the center of the hot zone. At the end of the oxidation period, the furnace was lowered and the sample cooled rather rapidly. During this operation the external scale became detached from the substrate allowing the formation of a porous scale within a few minutes. Therefore, these samples were not used for metallography.

Table I. Alloy Compositions (wt.%) as Determined by EDAX

Alloy designation	Fe	Mn	Cr
Fe–5Cr–2Mn	Bal	4.9	2.5
Fe–5Cr–6Mn	Bal	4.8	6.6
Fe–5Cr–10Mn	Bal	4.8	9.9
Fe–12Cr–2Mn	Bal	11.9	2.4
Fe–12Cr–6Mn	Bal	12.1	6.2
Fe–12Cr–10Mn	Bal	11.9	9.9
Fe–20Cr–2Mn	Bal	19.4	2.8
Fe–20Cr–6Mn	Bal	19.5	6.6
Fe–20Cr–10Mn	Bal	19.5	9.8

Metallographic samples were oxidized in a sealed, horizontal furnace using a flowing oxygen atmosphere. The oxidizing atmosphere was similar to that used in the kinetics experiments. Samples were suspended in an alumina boat, which was pushed into the hot zone of the furnace once the oxidizing temperature of $900 \pm 3°C$ was reached. On completion of the oxidation run, a dry argon gas flow was introduced in order to avoid further oxidation of the substrate in the event of external-scale detachment. The furnace was cooled to ambient temperature at a rate of about 100°C/hr. The flow rates of both oxygen and argon were measured at 100 ml/min.

Oxidized samples were analyzed by diffractometry employing Cu–K_α radiation. The samples were mounted in epoxy resin, metallographically prepared, and photographed. The samples were further examined using Energy Dispersive Analysis of x-rays (EDAX). In identifying the reaction products, the interplanar spacing for $MnCr_2O_4$ was taken from Yearian *et al.*,[11] where the lattice parameter ranged from 8.435–8.420 Å.

RESULTS

Kinetics plots for all alloys are shown in Figs. 1 and 2. The detailed results are presented separately for the different families of alloys. The kinetics measurements were plotted according to the parabolic rate equation

$$(\Delta W/A)^2 = k_p t + C \tag{1}$$

where $(\Delta W/A)$ is the weight gain per unit area formed in time, t, and k_p, C are constants. It was found in this way that two successive stages of parabolic kinetics were in effect. The rate constants formed from regression on Eq. (1) are listed in Table II. It is seen that the second-stage rate constant, $k_p(2)$, is about one order of magnitude greater than $k_p(1)$ for all alloys. The Fe–20Cr–10Mn alloy has an extra rate constant $k_p(3)$.

Cross-sections of the scales formed on the alloys are shown in Figs. 3–7. The identifications of the scale products formed on the alloys after 24 hr oxidation at 900°C are listed in Table III.

Low-Chromium Alloys: Fe–5Cr–*X*Mn and Fe–12Cr–*X*Mn

The six low-chromium alloys produced similar scale morphologies after 24 hr of reaction. Depending on the manganese content, the alloy formed either duplex or triplex scales. The duplex scale consisted of an outer α-Fe_2O_3 layer above an M_3O_4 layer. The triplex scales had similar constituents, with an additional exterior layer of $(Mn,Fe)_2O_3$ at the gas–scale interface, with the exception of Fe–5Cr–10Mn, which formed $MnFe_2O_4$. While the inner layer of M_3O_4, contained chromium, the α-Fe_2O_3 and $(Mn,Fe)_2O_3$

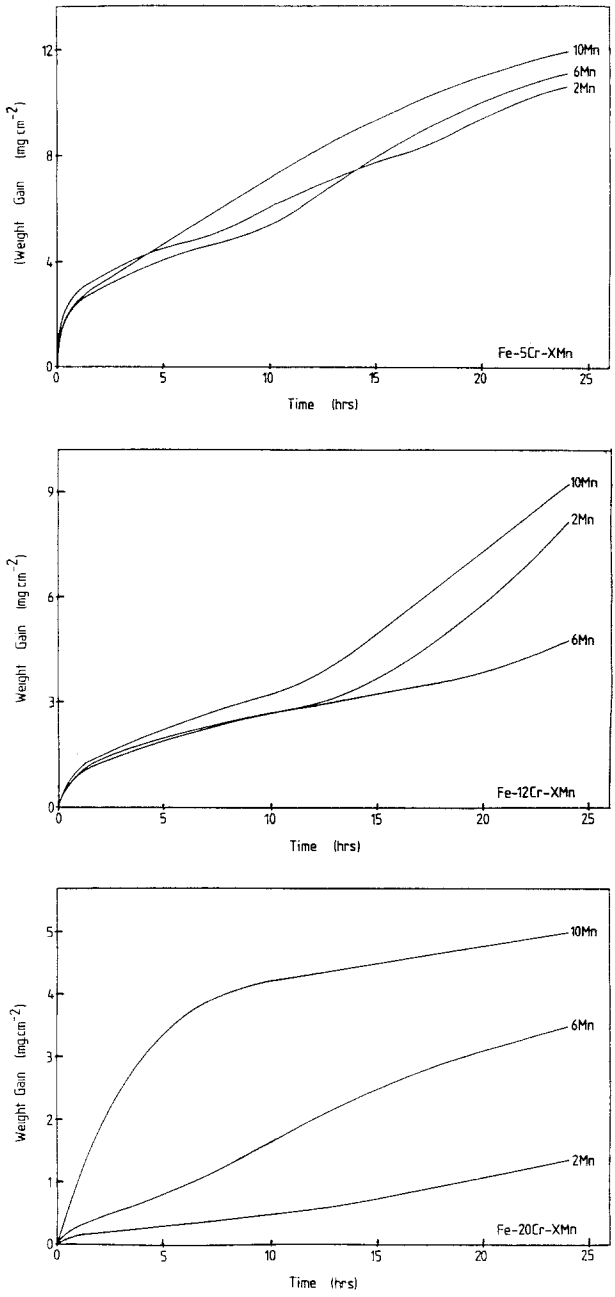

Fig. 1. Oxidation kinetics of Fe–Cr–Mn alloys oxidized at 900°C. (p_{O_2} = 26.7 kPa).

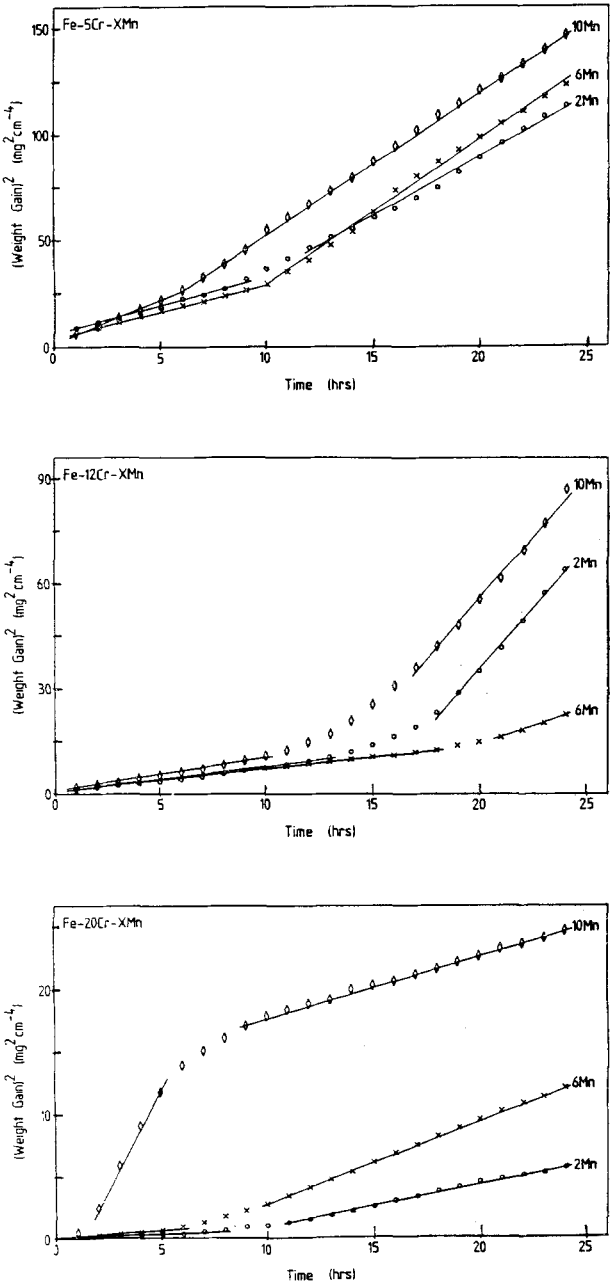

Fig. 2. Plots of $(\Delta W/A)^2$ vs. time for Fe–Cr–Mn alloys oxidized at 900°C. (p_{O_2} = 26.7 kPa).

Table II. Parabolic Rate Constants for the Oxidation of Fe–Mn,[17] Fe–Cr,[17] and Fe–Cr–Mn Alloys for 24 hr at 900°C in an Oxygen Pressure of 26.7 kPa[a]

Alloy	$k_p(1)$	$k_p(2)$
Fe–2Mn[b]	3.2×10^{-7}	2.5×10^{-7}
Fe–6Mn[b]	1.9×10^{-7}	1.2×10^{-7}
Fe–10Mn[b]	1.6×10^{-7}	1.0×10^{-7}
Fe–5Cr	8.3×10^{-10}	2.1×10^{-9}
Fe–12Cr	5.0×10^{-10}	6.6×10^{-10}
Fe–20Cr	8.9×10^{-12}	2.9×10^{-11}
Fe–5Cr–2Mn	8.9×10^{-10}	1.6×10^{-9}
Fe–5Cr–6Mn	7.5×10^{-10}	2.2×10^{-9}
Fe–5Cr–10Mn	1.2×10^{-9}	1.9×10^{-9}
Fe–12Cr–2Mn	2.1×10^{-10}	1.9×10^{-9}
Fe–12Cr–6Mn	2.1×10^{-10}	4.4×10^{-10}
Fe–12Cr–10Mn	2.9×10^{-10}	1.8×10^{-9}
Fe–20Cr–2Mn	1.6×10^{-11}	9.9×10^{-11}
Fe–20Cr–6Mn	2.8×10^{-11}	1.8×10^{-10}
Fe–20Cr–10Mn[c]	9.0×10^{-11}	7.7×10^{-10}

[a]Rate constants units: $g^2 \cdot cm^{-4} \cdot sec^{-1}$.
[b]6 hr oxidation.
[c]This alloy exhibited a third rate constant: $k_p(3) = 1.4 \times 10^{-10}\ g^2 \cdot cm^{-4} \cdot sec^{-1}$.

Table III. Oxide-Layer Constitution as a Function of Alloy Composition[a]

Alloy	Inner	Outer
Fe–5Cr–*X*Mn		
2Mn	$(Fe,Mn)_3O_4$	α-Fe_2O_3
6Mn	$(Fe,Mn)_3O_4$	α-Fe_2O_3
10Mn	$(Fe,Mn)_3O_4$	α-Fe_2O_3/$MnFe_2O_4$
Fe–12Cr–*X*Mn		
2Mn	$(Fe,Mn)_3O_4$	α-Fe_2O_3
6Mn	$(Fe,Mn)_3O_4$	α-Fe_2O_3/$(Mn,Fe)_2O_3$
10Mn	$(Fe,Mn)_3O_4$	α-Fe_2O_3/$(Mn,Fe)_2O_3$
Fe–20Cr–*X*Mn		
2Mn	—	$MnCr_2O_4$
6Mn (thin scale)	$Mn(Mn,Cr)_2O_4$	$(Mn,Cr)_2O_3$
6Mn (nodule)	M_3O_4/$(Cr,Fe)_2O_3$	$(Mn,Fe)_2O_3$/α-Fe_2O_3
10Mn (thin scale)	$Mn(Mn,Cr)_2O_4$	$(Mn,Cr)_2O_3$
10Mn (nodule)	M_3O_4/$(Cr,Fe)_2O_3$	$(Mn,Fe)_2O_3$/α-Fe_2O_3

[a]Bixbyite: $(Mn,Fe)_2O_3$; M_3O_4: $(Fe,Cr,Mn)_3O_4$.

phases did not contain any chromium. The cross-sections revealed that the third manganese-rich layer was thin and could be either discontinuous or continuous. No Mn_2O_3 was found on these alloys after 24 hr, but after a 30 min oxidation period Fe–12Cr–6Mn and Fe–12Cr–10Mn produced

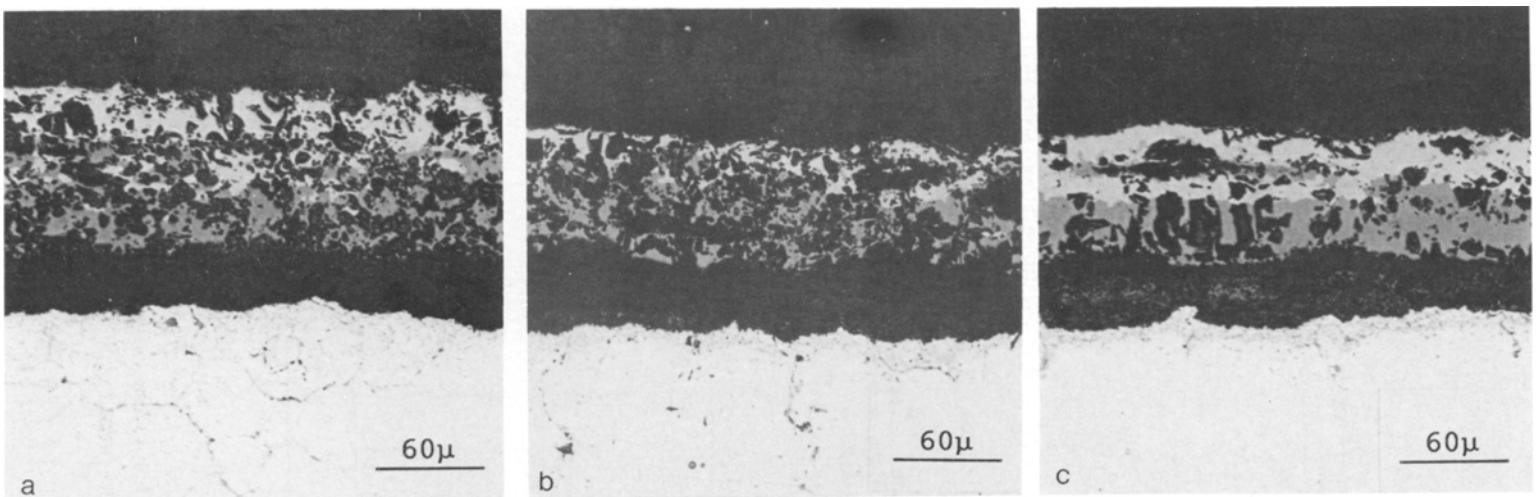

Fig. 3. Cross-sections of the bulky scales formed on Fe–5Cr–*X*Mn alloys after 24 hr at 900°C: (a) 2Mn; (b) 6Mn; (c) 10Mn.

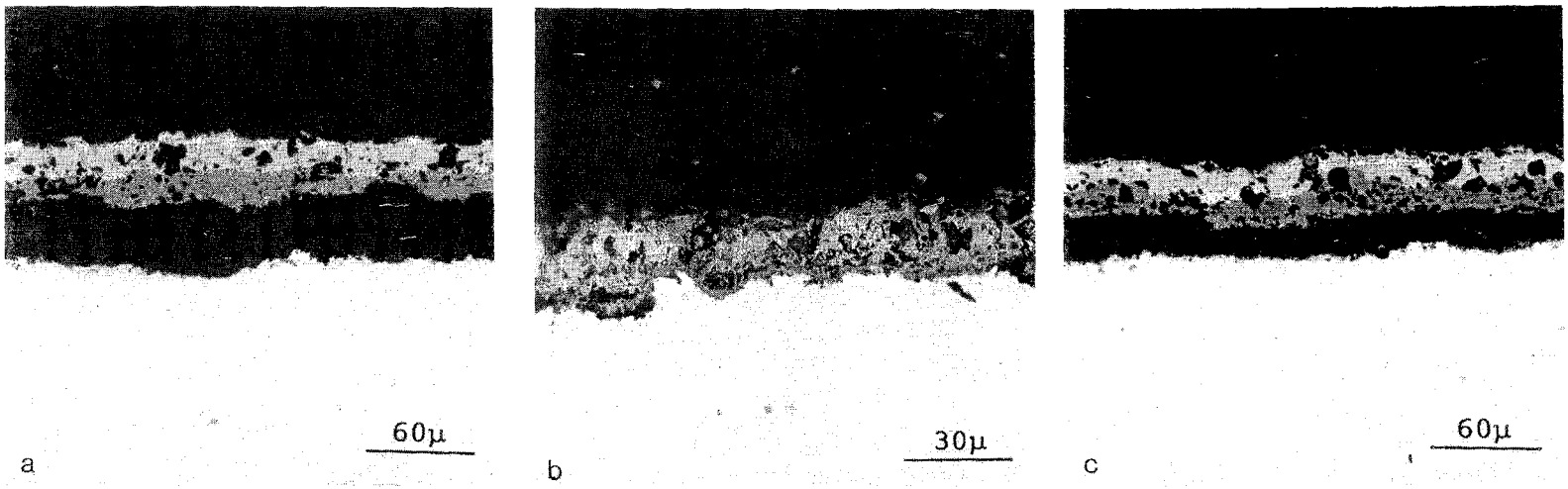

Fig. 6. Cross-sections of bulky scales formed on Fe–12Cr–*X*Mn alloys after 24 hr at 900°C: (a) 2Mn; (b) 6Mn; (c) 10Mn.

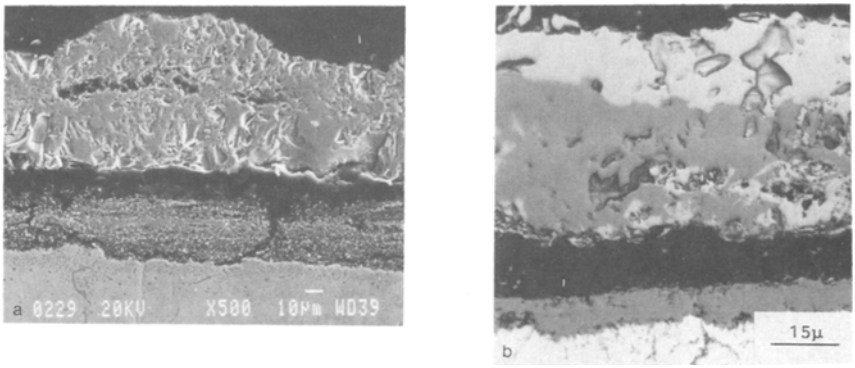

Fig. 4. Cross-section of porous oxide scale which formed upon cooling from 900°C, when the external scale was detached: (a) Fe–5Cr–10Mn, 24 hr oxidation; (b) Fe–5Cr–2Mn, 16 hr oxidation.

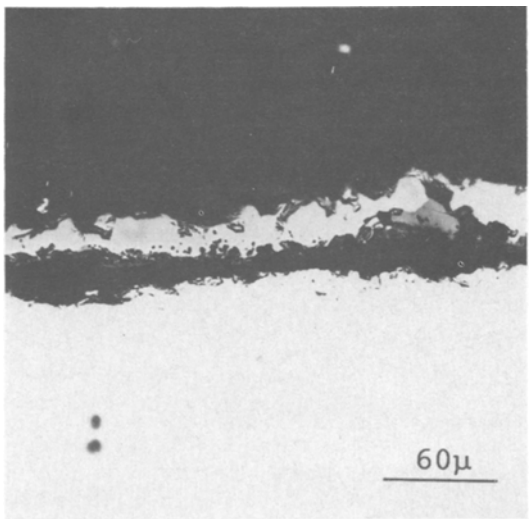

Fig. 5. Cross-section of α-Fe_2O_3 formed on Fe–5Cr–6Mn after 3 hr oxidation at 900°C.

Mn_2O_3. With exposure times greater than 2 hr, the Mn_2O_3 was replaced by $(Mn,Fe)_2O_3$.

The inner M_3O_4 layer was mainly Fe_3O_4 with dissolved manganese and chromium. For all these alloys, the manganese content in this layer was similar to that of the bulk alloy content. Chromium enrichment occurred at the base of this layer, although no separate chromite phase was observed.

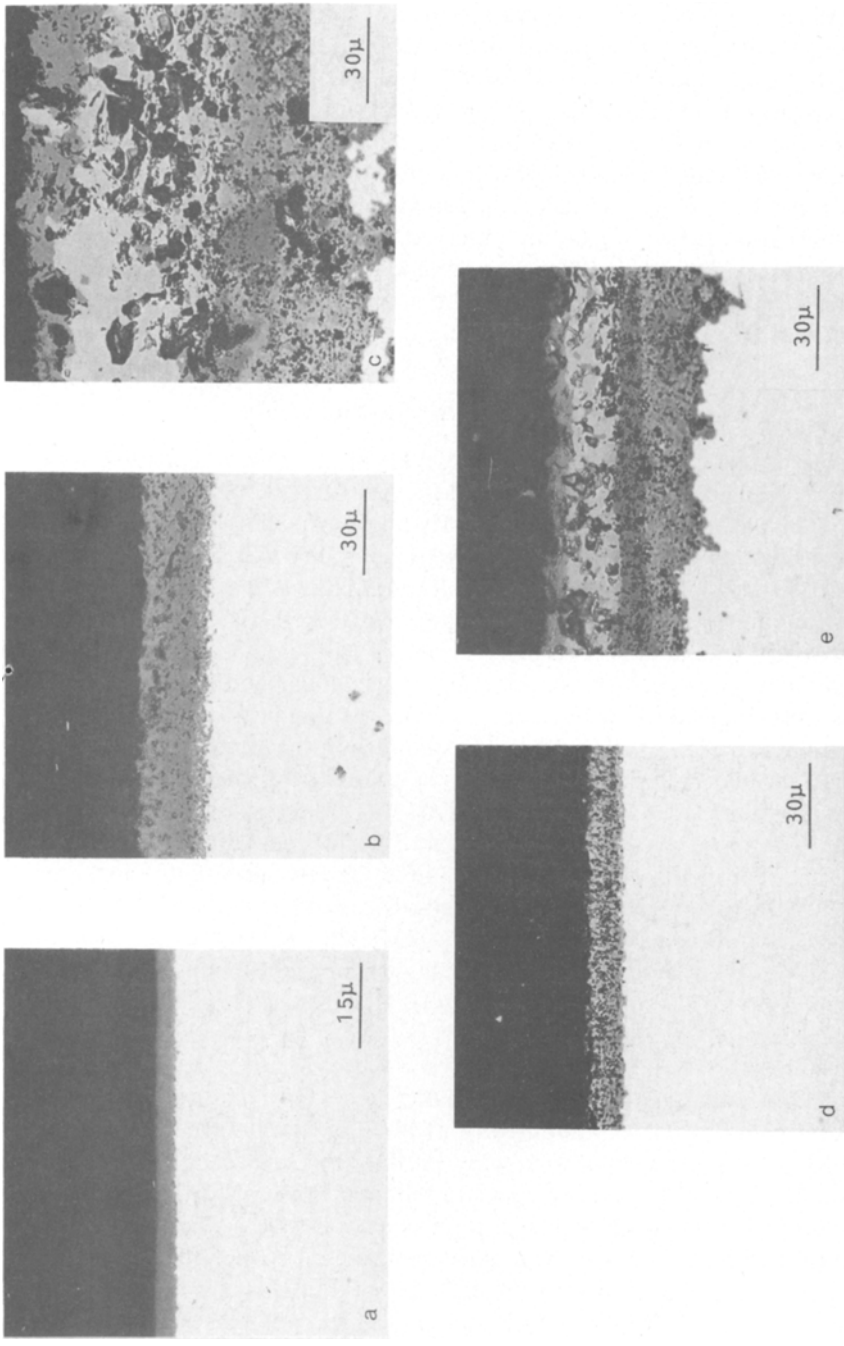

Fig. 7. Cross-sections of scales formed on Fe–20Cr–*X*Mn alloys after 24 hr at 900°C: (a) 2Mn; (b) 6Mn—thin scale region; (c) 6Mn—nodule region; (d) 10Mn—thin scale region; (e) 10Mn—nodule region.

All the alloys experienced a varying degree of internal oxidation, with the 5Cr alloys being severely attacked. Scale detachment in these alloys occurred during cooling, resulting in rapid oxidation of the underlying substrate, even during brief cooling periods, as shown in Fig. 4.

In the initial stage of reaction, these alloys all oxidized to produce a single-layered scale of M_2O_3, consisting mainly of α-Fe_2O_3. An example is shown in Fig. 5, where the scale is predominantly α-Fe_2O_3, although localized nucleation sites of Fe_3O_4 are observed. The formation of a continuous M_3O_4 layer at the alloy surface corresponded to the commencement of the second stage of parabolic kinetics. The subsequent rate was an order of magnitude greater than the initial rate.

High-Chromium Alloys: Fe–20Cr–*X*Mn

The cross-sections show that as the manganese content increased, nodule formation became prevalent. The 2Mn alloy formed a thin, single-phase, adherent scale of $MnCr_2O_4$, while the 6Mn and 10Mn alloys formed complex scales consisting of thin scale and nodule regions. The thin scale on the 6Mn and 10Mn alloys was duplex (see Table III). The nodules on these alloys consisted of two regions: an outer region made up of $(Mn,Fe)_2O_3$ and α-Fe_2O_3 layers and an inner two-phase region of M_3O_4 and Cr_2O_3. The Cr_2O_3 morphology was varied; it appeared as a continuous band in the middle of the nodule (Fig. 7e) in the 6Mn alloy, or as large fragments (Fig. 7c) as well as a thin layer along the nodule–alloy interface in the 10Mn alloy.

All the alloys studied exhibited two-stage oxidation kinetics. In the low-chromium alloys, the formation of M_3O_4 was preceded by the growth of M_2O_3. The growth rate of M_3O_4 was an order of magnitude greater than that for the growth of an M_2O_3 layer. Like the low-chromium alloys, the Fe–20Cr–*X*Mn series also exhibited stage-wise parabolic kinetics. The initial, slow reaction corresponded in the case of 2Mn alloy to the growth of single-layered $MnCr_2O_4$, and in the case of the higher-manganese alloys to a duplex scale of $(Mn,Cr)_2O_3$ on top of $MnCr_2O_4$. This first stage of reaction was very brief in the case of the 10Mn alloy, but lasted for several hours for the other alloys.

The second stage of reaction, on these high-chromium alloys corresponded to the formation and growth of nodules. Because the nodules are formed in a "nucleation and growth" process, the kinetics are not strictly parabolic. Nonetheless, an average parabolic rate constant, $k_p(2)$, is reported in Table II for this reaction stage, to provide a basis for comparison. It is clear that the rate increases with alloy manganese content. In the reaction times examined, the oxidation kinetics show a third, and slower, stage in the case of the 10Mn alloy, but not for the lower-manganese alloys. The

commencement of the third stage of reaction was found to be associated with the formation of an additional layer of Cr_2O_3 at the scale base. Apparently, this layer provides a degree of protection to the alloy.

DISCUSSION

Because the scale morphologies are so different, the discussion will be divided into two sections according to the chromium concentration of the alloy: low-chromium alloys (i.e., with levels of 5 and 12 wt.%) and high-chromium alloys (i.e., containing 20 wt.%).

Low-Chromium Alloys

The six alloys in this group formed scales which could be classed as duplex or triplex. As shown in Table III, the duplex scales formed on the low-manganese alloys, such as the 2Mn and 6Mn alloys containing 5Cr and the 2Mn alloy containing 12Cr. Triplex scales formed on the higher-manganese alloys; Fe–5Cr–10Mn, Fe–12Cr–6Mn, and Fe–12Cr–10Mn.

The duplex scales which formed on low-manganese alloys resembled in their morphology and phase constitution the scales formed on low-chromium Fe–Cr alloys, which oxidize to yield scales of Fe_3O_4 overlaid by Fe_2O_3.[15] On the other hand, binary low-manganese Fe–Mn alloys form scales which are similar to those found on iron: a triplex scale consisting of Fe_2O_3/Fe_3O_4/FeO, with all phases containing dissolved manganese.[16] Although the addition of manganese to iron expands the stability field of the manganowustite phase, the addition of chromium destabilizes this phase. If the alloy manganese/chromium ratio is high enough, the MO phase will be stabilized, as has been reported for an Fe–17.8Mn–9.5Cr alloy.[7] For the alloys studied in the present work, however, the ratio is always lower and the MO phase is never produced.

The triplex scales developed on the higher-manganese alloys were similar to those formed on low-manganese alloys, but contained an additional layer of cubic oxide at the gas–scale interface. This cubic oxide contained no chromium, and was identified as bixbyite—$(Mn,Fe)_2O_3$—on the 12Cr alloys, but as $MnFe_2O_4$ spinel on Fe–5Cr–10Mn.

The formation of bixbyite results from partial replacement by iron cations of manganese cations in cubic α-Mn_2O_3. The phase diagram for this system[12] reveals limited intersolubility of Fe_2O_3 and Mn_2O_3. At 900°C, the solubility of Mn_2O_3 in Fe_2O_3 is 15 wt.%, while the solubility of Fe_2O_3 in Mn_2O_3 is almost 50 wt.%. The phase-equilibrium work also showed that at temperatures of 900°C and above, the M_3O_4 phase was starting to be the more stable oxide. Of course, the presence of chromium can alter the relative

stabilities of the oxides. The present results indicate that it favors the formation of bixbyite.

Unlike the alloys studied in the present work, an Fe–17.8Mn–9.5Cr alloy oxidized to produce a layer of Mn_2O_3 at the gas–scale interface.[7] In the present study, no Mn_2O_3 could be found on alloys oxidized for 2 hr or longer. However, the Fe–12Cr–6Mn and Fe–12Cr–10Mn alloys did have Mn_2O_3 at their scale exterior after a 30 min oxidation period. It was found by observing the change in *d*-spacing of the Mn_2O_3 diffraction lines, that this phase was replaced by $(Mn,Fe)_2O_3$ during subsequent reaction. This initial formation of Mn_2O_3 is attributed to the high diffusion coefficient of manganese in the alloy, and its high oxygen affinity.[2,14] The compositional change from Mn_2O_3 to $(Mn,Fe)_2O_3$ occurs as the alloy becomes depleted in manganese, and the increase in iron activity relative to that of manganese leads to substitutional diffusion of iron into the Mn_2O_3. Evidently, the manganese activity in the scale on the Fe–17.8Mn–9.5Cr alloy[7] was maintained at a value high enough to prevent this substitutional dissolution process.

The underlying oxide in the scales on all low-chromium alloys was Fe_3O_4 containing dissolved manganese and chromium. The Fe–Mn–O and Fe–Cr–O phase diagrams[7] show that significant quantities of chromium and manganese are soluble in Fe_3O_4 at 900°C. The extent of dissolved manganese in the scale depended on the manganese content of the alloy. However, there was an enrichment of manganese at both the outer–inner oxide layer and alloy-scale boundaries, especially in the low-manganese alloys. Similarly, there was a steady increase in the amount of chromium in Fe_3O_4 toward the alloy-scale boundary. The shape of these concentration profiles cannot be analyzed without detailed knowledge of the M_3O_4 solution thermodynamics.

In all scales, the thicknesses of the two major oxides (α-Fe_2O_3 and M_3O_4) were almost equal, except in the case of Fe–12Cr–6Mn. The scale on this alloy consisted mainly of α-Fe_2O_3 with a very thin M_3O_4 layer. The difference in morphology was reflected in the oxidation kinetics, and this alloy was the most oxidation-resistant of the low-chromium alloys.

It is useful to compare the oxidation rates of these alloys with those of binary Fe–Cr alloys. Extensive data on these latter alloys is available from the works of Lai *et al.*,[15] Mortimer and Sharp,[18] and Wood and Whittle,[19] but not at the alloy compositions and temperatures appropriate to present purposes. Accordingly, additional experiments were carried out on binary alloys. The results were consistent with those of others[15,18,19] and are shown in Table II.

The addition of 2Mn or 6Mn to Fe–5Cr is seen in Table II to have very little effect on either stage of the kinetics. This is consistent with the observations that scale morphologies are the same, and that manganese incorporation into the scale was at a low level. The addition of 10Mn to Fe–

5Cr led to the formation of an additional layer, and to a somewhat faster initial rate. The long-term oxidation rate was essentially unchanged, indicating that the diffusion behavior of the M_3O_4 layer is not significantly affected by manganese incorporation.

Adding manganese to Fe–12Cr has a mildly beneficial effect on the first-stage rate constant, corresponding to a slower growth rate of the Fe_2O_3 layer. After formation of an M_3O_4 layer, however, the subsequent rate was faster for the ternary alloys, with the exception of Fe–12Cr–6Mn. In this latter case, it is likely that the steady-state reaction rate has not been achieved (see Fig. 1). The formation of the inner M_3O_4 layer on this alloy was delayed for reasons which are still not understood, as the outer M_2O_3 layer formed had a similar composition to that of corresponding layers on the other ternary alloys.

High-Chromium Alloys

The scale produced on the 2Mn alloy was a thin, adherent scale which was not blistered, and the alloy-scale boundary was planar. The scale was identified by EDAX as consisting of an $MnCr_2O_4$ layer on top of a thin manganese-containing Cr_2O_3 inner layer. This result is in agreement with earlier reports[1,2,11] of the effect of small manganese additions on chromia-forming Fe–Cr alloys. It is a consequence of the permeability to manganese of the Cr_2O_3 layer.

The thin-scale region on the 6Mn and 10Mn alloys was also enriched in manganese at its exterior surface. The degree of enrichment was much greater, however, and an outer layer of cubic $(Mn,Cr)_2O_3$ formed at the gas-scale interface. This increased manganese enrichment results from the higher alloy manganese activities and the relatively rapid diffusion of manganese through the inner chromia layer. This finding differs from a recent report that the scale formed on Fe–26Cr–5Mn contained Mn_3O_4 and $MnCr_2O_4$ above a layer of Cr_2O_3.[1]

The manganese content in the outer thin-scale layer on the 6Mn and 10Mn alloys was identified as Mn_2O_3 containing dissolved chromium. The outer layer contained no more than 15 wt.% chromium and, the inner layer of the thin scale contained up to 45 wt.% manganese. The oxide intersolubilities[7,13] at 900°C, are approximately 25 wt.% Cr_2O_3 in Mn_2O_3 and 15 wt.% Mn_2O_3 in Cr_2O_3. The outer-layer composition is consistent with these limits, but the inner layer is beyond the solubility limit of Mn_2O_3 in Cr_2O_3. However, it was possible that this inner layer was a manganese-rich $MnCr_2O_4$ spinel. This is in agreement with the phase diagram,[13] which indicates that the spinel contains up to 60 wt.% Cr_2O_3.

The growth rates of the thin scales formed on the alloys in the first stage of reaction were found to increase with alloy manganese content and were all higher than the oxidation rate of Fe–20Cr. With an increase in the alloy manganese activity, there is a greater driving force to form a manganese-rich oxide. This results in a higher manganese concentration in the inner chromium-rich layer, and in more rapid growth of the outer manganese-rich layer (spinel or $(Mn,Cr)_2O_3$). The effect is quite large, as seen in the brief initial period of oxidation observed for Fe–20Cr–10Mn, where the rate constant was an order of magnitude higher than for the lower-manganese alloys. However, this effect is seen to be unimportant when compared with the nodule-growth phenomenon.

The most destructive feature of the oxidation reaction in this alloy series was the outbreak of nodule growth. This is not surprising, as manganese is incorporated into the chromia layer, lowering its overall protectiveness.[3] Nodule formation was associated with breakdown of the protective chromia-based layer, adjacent to the alloy. The inner layer of this scale region was penetrated by the rapid, outward diffusion of manganese and iron cations, at locations favorable to diffusion. As manganese and iron cations have similar ionic radii, the replacement of manganese by iron without significant distortion to the manganese-rich $MnCr_2O_4$ structure is likely. This was shown quite clearly by analysis of the nodule pictured in Fig. 7e. The continuous layer in the middle of the nodule was found to be chromium-rich $(Cr,Fe,Mn)_2O_3$.

The rapid diffusion of both iron and manganese cations through the initially formed thin scale resulted in the formation of iron-rich nodules. The high oxygen affinity of manganese enhanced the development of $(Mn,Fe)_2O_3$ at the nodule–gas interface. The chromium-rich, central band in the nodule shown in Fig. 7e, which was part of the inner manganese-rich $MnCr_2O_4$ layer, had been depleted of manganese. It is thought that the manganese in this layer had diffused to the nodule–gas interface during nodule growth.

The formation of manganese-rich $MnCr_2O_4$ in the thin scale prior to nodule growth decreases the chromium and manganese content of the substrate alloy. When a nodule forms, it initially grows into and consumes this chromium-and manganese-depleted region, forming iron-rich $(Fe,Cr,Mn)_3O_4$. The advancing nodule–alloy interface eventually reaches a location at which high chromium levels exist, and $(Cr,Fe)_2O_3$ is formed. The inward growth of the nodule is slowed when a continuous chromia-based layer forms at the nodule–alloy interface. This healing layer is not Cr_2O_3, but possibly chromium-rich $(Cr,Fe)_2O_3$ with some dissolved manganese. The oxidation kinetics show a much reduced rate in the latter stage of reaction as a result of this healing-layer formation. This is clearly apparent for the Fe–20Cr–10Mn alloy, and a third (slow) parabolic stage of reaction is observed.

Nonetheless, the rate constant is an order of magnitude greater than for an Fe–20Cr alloy,[17] because manganese-rich oxides are formed.

Alloy oxidation rates are compared in Table II with those of binary Fe–Cr alloys, containing similar chromium levels.[15,17–19] It is apparent that the addition of manganese increases the oxidation rate, although the magnitude of the increase depends on the chromium content. The change in rate is marginal in the 5Cr alloys, but the 20Cr alloys exhibited a significant increase in both rate constants.

Other Fe–Cr–Mn alloys studied[7–9] showed rather different oxidation rates because of their higher manganese content. The alloys Fe–9.5Cr–17.8Mn,[7] Fe–19.6Cr–15.1Mn[8] and Fe–18Cr–12.3Mn[9] produced at 900°C, rate constants of $5 \times 10^{-8}\ g^2 \cdot cm^{-4} \cdot sec^{-1}$, $4 \times 10^{-10}\ g^2 \cdot cm^{-4} \cdot sec^{-1}$ and $7.3 \times 10^{-10}\ g^2 \cdot cm^{-4} \cdot sec^{-1}$, respectively. These rates are higher than that of Fe–20Cr–10Mn because of the higher manganese content and perhaps also due to the presence of impurities. These experiments are complicated by the fact that removal of manganese from the alloy region beneath the scale results in the formation of a ferritic sublayer in an otherwise austenitic alloy.

The alloys studied in the present work all exhibited two-stage kinetics which reflected the growth of multilayered scales. The formation of multilayered scales was associated with compositional changes at the advancing alloy–scale interface. The low-chromium alloys exhibited high oxidation rates as nonprotective iron-rich oxides formed. The first stage of reaction reflected the growth of Fe_2O_3, while the second stage corresponded to the formation of Fe_3O_4. The latter phase contained dissolved manganese and chromium. The high-chromium alloys exhibited lower oxidation rates. The initially formed thin scales grew slowly, but were subsequently penetrated by iron and manganese cations which formed iron-rich nodules. In the case of the 10Mn alloy, the formation of a healing layer at the base of the nodule resulted in a lower third-stage oxidation rate.

CONCLUSIONS

The oxidation of nine ternary iron–chromium–manganese alloys demonstrated that the presence of manganese had an adverse effect on the oxidation resistance of iron–chromium alloys. Even when the chromium content was sufficiently high to permit the formation of Cr_2O_3 on iron–chromium alloys, it was inadequate in a ternary alloy to prevent the formation of a spinel. The alloys with low-chromium contents, 5 and 12 wt.%, formed stratified bulky scales which had a propensity to spall during cooling. The scales on these low-chromium alloys contained an outer M_2O_3 phase, which was usually bixbyite—$(Mn,Fe)_2O_3$—and α-Fe_2O_3. The inner layer

consisted of Fe_3O_4 with varying amounts of dissolved manganese and chromium. These alloys were also internally oxidized. The higher-chromium alloys formed a mixture of Cr_2O_3 and spinel, which decreased the rate of oxidation. However, the presence of manganese initiated nodule growth, and with a frequency which increased with manganese content.

ACKNOWLEDGMENTS

One of us (A. L. Marasco) would like to acknowledge the financial support given by the Australian Government and Alcan Australia, Ltd.

REFERENCES

1. F. H. Stott, F. I. Wei, and C. A. Enahoro, *Werkst. Korros.* **40**, 198 (1989).
2. D. Caplan, P. E. Beaubien, and M. Cohen, *Trans. AIME.* **233**, 766 (1965).
3. R. K. Wild, *Corrosion* **17**, 87 (1977).
4. D. L. Douglass and J. S. Armijo, *Oxid. Met.* **3**, 185 (1971).
5. G. N. Irving, J. Stringer, and D. P. Whittle, *Oxid. Met.* **8**, 393 (1974).
6. D. L. Douglass and J. S. Armijo, *Oxid. Met.* **2**, 207 (1970).
7. D. L. Douglass, F. Gesmundo, and C. de Asmundis, *Oxid. Met.* **25**, 235 (1986).
8. D. L. Douglass and F. Rizzo-Assuncao, *Oxid. Met.* **29**, 272 (1988).
9. F. Gesmundo, C. de Asmundis, G. Battilana, and E. Ruedl, *Werkst. Korros.* **38**, 368 (1987).
10. J-G. Duh and J-W. Lee, *J. Electrochem. Soc.* **136**, 847 (1989).
11. H. J. Yearian, E. C. Randell, and T. A. Longo, *Corrosion* **12**, 55 (1956).
12. B. Mason, *Am. Mineral.* **29**, 67 (1944).
13. D. H. Speidel and A. Muan, *J. Am. Ceram. Soc.* **46**, 577 (1964).
14. O. Kubaschewski and B. E. Hopkins, *Oxidation of Metals and Alloys* (Butterworths, London, 1962), p. 236.
15. D. Lai, R. J. Borg, M. J. Brabers, J. D. Mackenzie, and C. E. Birchenall, *Corrosion* **17**, 109 (1961).
16. P. R. S. Jackson and G. R. Wallwork, *Oxid. Met.* **20**, 1 (1983).
17. A. L. Marasco (unpublished work).
18. D. Mortimer and W. B. A. Sharp, *Br. Corros. J.* **3**, 61 (1968).
19. G. C. Wood and D. P. Whittle, *Corros. Sci.* **7**, 763 (1967).